

13,04

Combine XPS- and AFM Study of Silicon Oxide Film with Zinc Impurity for ReRAM Devices

© V.V. Privezentsev¹, A.P. Sergeev¹, A.A. Firsov¹, D.A. Kiselev²

¹Federal State Institution „Federal Scientific Center Scientific Research Institute of System Analysis of the Russian Academy of Sciences“, Moscow, Russia

²National University of Science and Technology MISiS, Moscow, Russia

E-mail: v.privezentsev@mail.ru

Received January 21, 2022

Revised January 21, 2022

Accepted January 22, 2022

The composition, structure and properties, as well as the current-voltage characteristics of a layered structure consisting of two 50 nm thick amorphous SiO₂ films deposited by electron beam evaporation, between which a Zn film with a thickness that varied from 100 nm to 50 nm was deposited. Then these structures were annealed in air in the temperature range from 300 up to 400°C with a step of 50°C for 30 min. Planar electrodes with different configuration were used. They were made from gold, platinum and aluminum. It was found that after deposition on the sample surface, a granular structure with a grain size of 50–100 nm of SiO₂ composition was formed. After annealing at 400°C, the sample roughness decreases from 25 nm after deposition to 10 nm, and the grain size in plan increases to 100–200 nm. For films annealed at 400°C the current-voltage characteristics with hysteresis were obtained.

Keywords: silicon oxide film, zinc impurity, electron beam evaporation, annealing, nanoclusters, ZnO.

DOI: 10.21883/PSS.2022.07.54594.280

1. Introduction

Currently, resistive switching induced by an electric field is studied in many materials [1–3]. Resistive switching based random access memory (ReRAM) based on metal oxide materials along with a simple geometry and a wide choice of such materials (NiO, TiO₂, HfO₂) showed high performance, including high switching speed of several ns, low operating current of the order of nA, scalability in the nanometer range, and potential memory of several bits [4–6]. Recently, it has been shown that thin films of Zn-doped amorphous SiO_x (the so-called ZSO-films) are promising materials for ReRAM devices due to the compatibility of their technology with CMOS-technology [7]. Such films were obtained in both single-layer [8] and multilayer [9] versions. They had current-voltage (C-V) characteristics that varied from diode to memristor depending on the concentration of Zn and/or ZnO_x nanoclusters (NCs) and the change in the DC voltage applied to the silicon oxide film. The presence of Zn and/or ZnO_x NCs in silicon oxide, i.e., generally speaking, accumulations of Zn-containing defects [10] was proposed as the reason for this behavior. In this connection, it becomes necessary to study Zn-doped SiO_x films, their structure and properties, as well as their C-V characteristics with the hysteresis effect. It should be noted that silicon oxide is a widely used material in microelectronics, and zinc oxide is a material with a wide bandgap of 3.37 eV, which can provide a higher ohmic resistance value for the memristor in high resistance mode

(LRS), which will positively affect the stability of devices. In ReRAM devices based on ZSO-films, a possible hopping mechanism of conduction in the low-resistance state [11] has been noted. In this article, we study silicon oxide films doped with zinc obtained by electron-beam evaporation and subsequent annealing in an oxidizing environment at elevated temperatures.

2. Samples and experimental procedure

In this article, we study the composition, structure, and properties, as well as the C-V characteristics of a layered structure consisting of SiO₂ films with a thickness of 120 nm deposited by electron beam evaporation, over which a Zn film with a thickness varied from 10 to 50 nm was deposited. A protective silicon oxide film up to 10 nm thick was sometimes deposited over it. Then these structures were sequentially annealed in air in the temperature range from 300 to 450°C with a step of 50°C for 30 min at each step. We used planar electrodes made of deposited gold, platinum, and aluminum.

The films were deposited using an electron beam setup L-560Q (Leybold-Heraeus) with an oil-free pumping system and an electron gun that directly deposited materials from a copper crucible cooled by running water. Preliminarily chemically cleaned quartz substrates 1 mm thick were heated to 250°C for degassing under vacuum 10⁻⁶ mm · Hg, and then the temperature was lowered

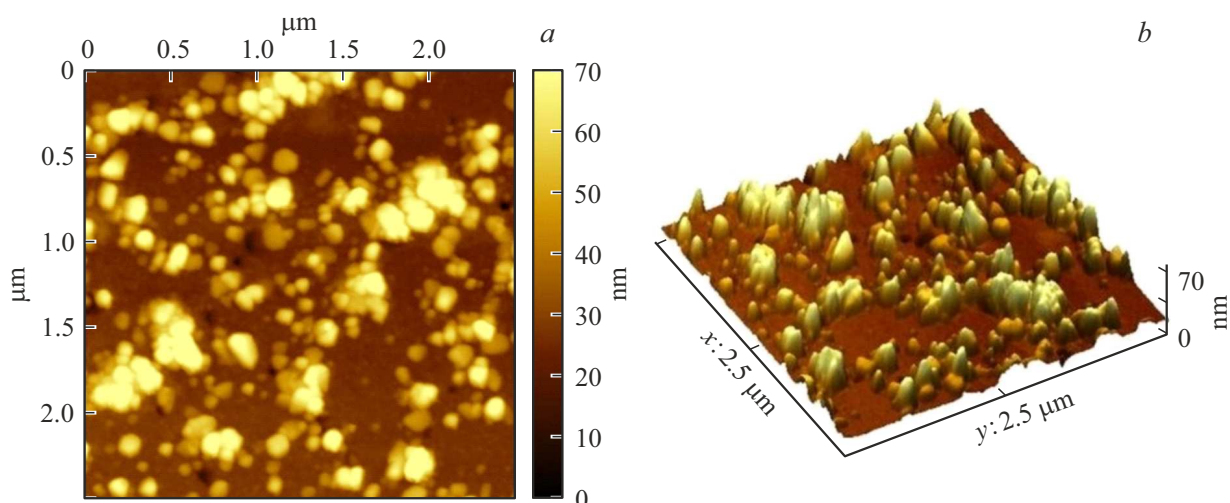


Figure 1. 2D (a) and 3D (b) AFM images of the SiO₂ film surface after sputtering.

to room temperature. Layers of fused silica, zinc and fused silica were deposited alternately. Deposition of SiO₂ layers was carried out at a pressure of $2 \cdot 10^{-5}$ mm · Hg, accelerating voltage of 11 kV, and a power of about 500 W. Deposition rate of SiO₂ was 1.5–2 A/sec, deposition rate of Zn — 30 A/sec with an accuracy of ± 0.1 Å with control by quartz monitor „Inficon“. Thicknesses of deposited layers: zinc — 10–50 nm, SiO₂ — 120 nm with accuracy ± 0.5 nm. In the case of Zn deposition, ChDA grade zinc granules were used as sputtering targets. When depositing the SiO₂ film, we used material made of KU-1 grade optical quartz. The total deposition time of the layers was approximately 60 min. After appropriate annealing, metal electrodes made of Au, Pt, and Al with a thickness of about 100 nm were deposited onto the applied Zn and SiO₂ layers.

The sample surface morphology was studied using a scanning probe microscope MFP-3D Stand Alone (Asylum Research, USA) in the semicontact mode (AC Air Topography), and the surface potential signal was recorded in the Kelvin mode. During measurements, we used HA_{NC}/Pt cantilever (Tipsnano, Estonia) with a stiffness of 3.5 N/m and a resonant frequency of free vibrations of 140 kHz. The obtained images were processed using the Gwyddion [12] program.

The chemical state of the elements of the obtained films was studied using X-ray photoelectron spectroscopy (XPS), as well as Auger electron spectroscopy (AES) with depth profiling. The aims of the study were the chemical state of impurities and their concentration profiles. The studies were carried out using a PHI 5500 Versa Probe II XPS spectrometer. The excitation source was X-ray monochromatic Al-K α -radiation ($h\nu = 1486.6$ eV) with power of 50 W, the beam diameter was 200 μ m, and the analysis area was 600 \times 200 μ m. The study used a neutralizer. Survey spectra were recorded in the range 0–1100 eV at the analyzer's transmission energy

$E_{\text{pass}} = 117.4$ eV with a step of 1 eV/step. The high resolution XPS spectra of Zn2p_{3/2} and OES Zn L3M45M45 were measured at $E_{\text{pass}} = 23.5$ eV with a step of 0.2 eV. The binding energy scale (E_B) was corrected using the spectrum of the Zn2p_{3/2} line with energy of 1022 eV. The chemical state of zinc was determined using the Auger parameter (AP) $\alpha' \equiv E_{\text{kin}}(\text{Zn-L3M45M45}) + E_B(\text{Zn2p}_{3/2})$, and $E_{\text{kin}}(\text{Zn-L3M45M45}) = 1486.6 - E_B(\text{Zn-L3M45M45})$. The atomic concentrations of elements were determined by the method of relative elemental sensitivity factors using survey XPS spectra, and the concentrations were determined based on the measured integral intensities of the following lines: C1s, O1s, Si2s, Zn2p_{3/2}. The E_B binding energy scale was calibrated using the Au4f lines with energy of 84.0 eV and Cu2p_{3/2} lines with energy of 932.6 eV. The error in determining the binding energies (and kinetic energy) was $\Delta E = \pm 0.2$ eV. For layer-by-layer analysis, the substrate was etched with Ar⁺ ions with energy of 2 keV, while the etching raster was 2 \times 2 mm, and the etching rate in this mode was 9 ± 1 nm/min.

3. Results and discussion

3.1. Analysis of the surface topology on an atomic force microscope

Figure 1 shows 2D- and 3D-images of the silicon oxide surface after zinc film deposition. The surface is characterized by the following parameters: Ra = 0.14 nm, and Rms = 8.0 nm. It follows from Fig. 1 that there are hillock on the surface up to 46.8 nm in height, having a lateral size of the order of 100 nm.

Figure 2 shows 2D (a) and 3D (b) AFM images of the surface of a silicon oxide film doped with zinc after annealing at 400°C.

The surface is characterized by the following parameters: the average value of the surface heterogeneity is

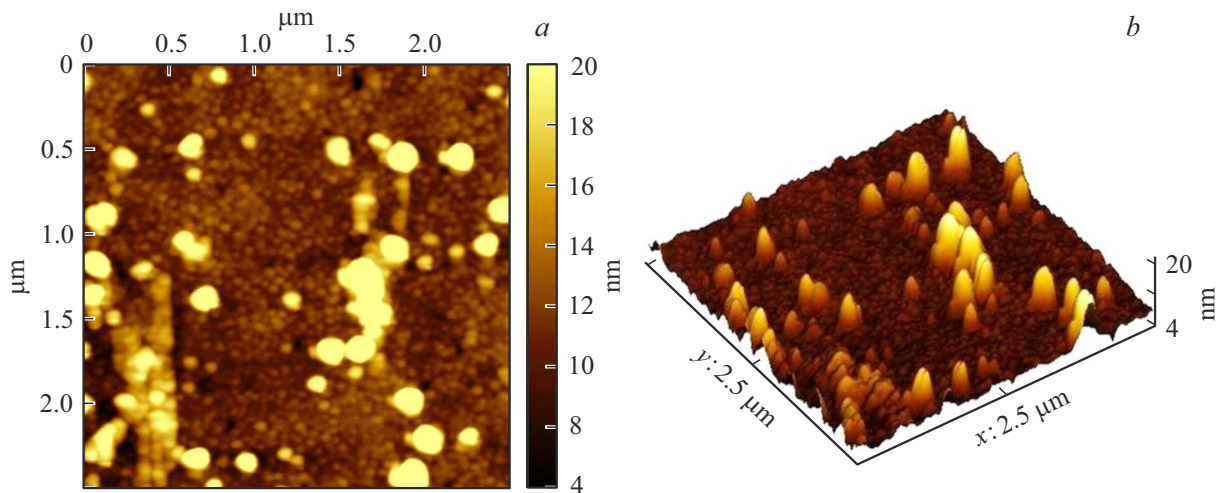


Figure 2. 2D (a) and 3D (b) AFM images of SiO₂ films after annealing at 400°C.

Ra = 0.45 nm, Rms = 0.36 nm. It follows from a comparison of the data in Figs. 1 and 2 that the surface roughness of the sample slightly increased after annealing from its state after deposition. Regarding the dimensions of surface heterogeneity in the plane, it can be noted that they also slightly increased, i.e. the surface is structured. We attribute such in-plane surface structuring to the formation of latent regions inside the silicon oxide film after annealing, which is accompanied by the formation of zinc and/or its oxide NCs. In this case, diffusion of Zn to the sample surface is possible, which is accompanied by the formation of its accumulations near the surface, which create irregularities on the surface itself. It is also possible for zinc to escape into the surrounding atmosphere with the formation of surface pores of small sizes (less than 5 nm).

Roughness distribution after deposition and after annealing at 400°C is shown in Fig. 3. It follows from a comparison of the 1 and 2 curves in Fig. 3 that the silicon oxide film surface roughness slightly decreased after annealing from its state after deposition. After annealing at 400°C, the sample surface is structured (Fig. 2): both large light spots with a size of about 100 nm and a fine-grained structure of darker color with a grain size of 20–50 nm, as well as individual pores appear on it. Regarding the dimensions of surface heterogeneity in the plane, it can be noted that they also increased, i.e. the surface is structured. We associate such surface in-plane structuring with the formation of latent regions inside the quartz matrix. For statistical processing of the roughness distribution in the sample plane, we used the formula for the probability density function of a random variable, the logarithm of which is normally distributed in Origin. The standard deviation for the film after deposition was 0.23 nm, and after annealing 0.19 nm.

Figure 4 shows AFM images of the SiO₂ film in the Kelvin mode after annealing at a temperature of 400°C; moreover, Figure 4, a shows the topography of the surface,

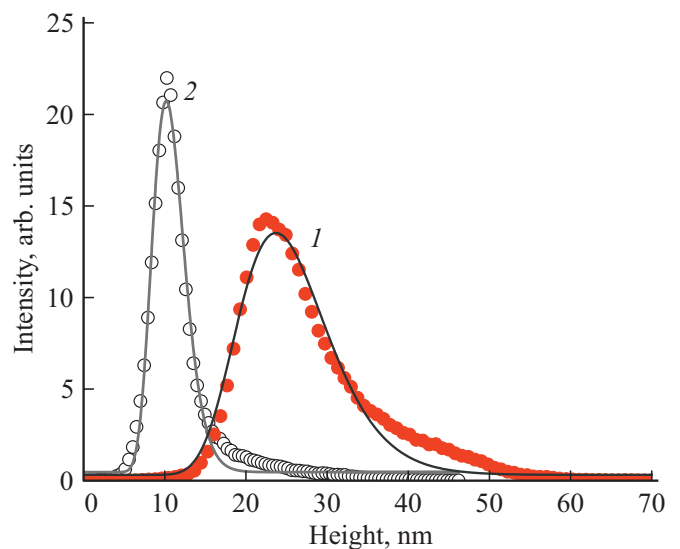


Figure 3. Film surface roughness distributions after deposition (1) and after annealing at 400°C (2). Points are experimental data; lines are approximation.

Figure 4, b — the surface potential. At the surface potential, heterogeneities are clearly visualized, which have a lower signal level compared to the background one, which can be attributed to the formation of Zn nanoparticles on the surface of the SiO₂ film after annealing. In this case, the larger the particle size, the more intense the signal of the surface potential of these heterogeneities, recorded in the Kelvin-mode.

Figure 4, c shows the surface image of a SiO₂ film doped with Zn after annealing at 400°C. Particles are „filled with“ pink color at a height of 20 nm, which is necessary to construct a histogram of particle diameter distribution in the plane in the film under study (Fig. 4, d). According to the statistics (using the formula of the probability density

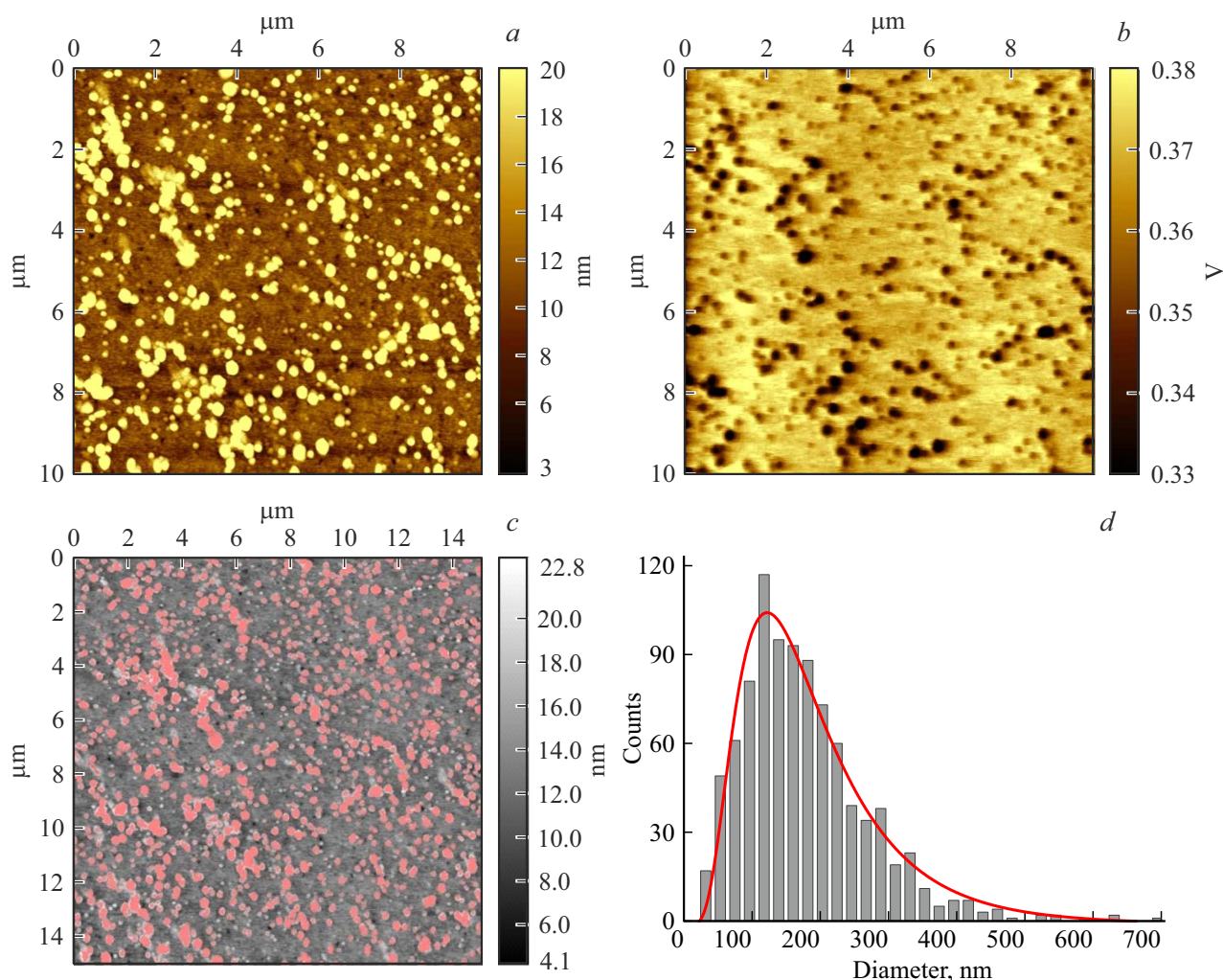


Figure 4. AFM images of a SiO_2 film doped with Zn in the Kelvin mode after annealing at 400°C : topography (*a*) and surface potential (*b*). Surface image (particles are „filled with“ pink color) (*c*) and particle size distribution histogram (*d*).

function of a random variable whose logarithm is normally distributed, the curve in Fig. 4,*d*), the average particle diameter was 166 nm, the standard deviation was 0.55 nm.

3.2. XPS-studies

Figure 5 shows survey XPS-spectra for the sample after deposition (*a*) and after etching for 5 min (at a depth of 45 nm) (*b*).

Figure 5,*a* shows a survey XPS-spectrum on the surface (0 nm). On this spectrum one can distinguish (from left to right) XPS-levels of zinc $\text{Zn}2p_1$ and $\text{Zn}2p_3$ and Auger oxygen level $\text{O}^- \text{KLL}$; Auger zinc levels $\text{Zn-LMM}2$, $\text{Zn-LMM}3$, XPS-level of oxygen $\text{O}1s$, Auger zinc levels Zn-LMM and $\text{Zn-LMM}1$; XPS-level of carbon $\text{C}1s$; XPS-levels of silicon $\text{Si}2s$ and $\text{Si}2p$ and zinc $\text{Zn}3s$ and $\text{Zn}3p$.

Figure 5,*b* shows the survey XPS-spectrum after 7 min etching (at a depth of 63 nm) in the same analysis region. It can be seen (from left to right) the Auger oxygen level $\text{O}^- \text{KLL}$; XPS-level of oxygen $\text{O}1s$, weak XPS-level

of carbon $\text{C}1s$, XPS levels of silicon $\text{Si}2s$ and $\text{Si}2p$ and XPS-level of oxygen $\text{O}2s$.

Figure 6,*a* shows the XPS-spectrum for the $\text{Zn}2p_{3/2}$ line in high resolution. It follows from this that the energy $E_B = 1020.7 \text{ eV}$ corresponds to the XPS-signal maximum on the substrate surface. With an increase in the depth of analysis to 18 nm, the signal increases and its maximum is already at the energy $E_w = 1021.3 \text{ eV}$. With a further increase in the depth of analysis, the XPS signal decreases, and the position of its maximum shifts at an analysis depth of 31.5 nm to the value of the binding energy $E_B = 1021.5 \text{ eV}$. A decrease in the binding energy for the $\text{Zn}2p_{3/2}$ line indicates a change in the charge state of zinc towards an increase in its positive value, in other words, in the depth of the substrate, zinc is in more oxidized state than on the surface.

Figure 6,*b* shows the Auger profiles for the Zn L3M45M45 transition. It follows from the figure that as the depth of analysis increases, the signal maximum first increases from 0 nm (surface) to a depth of 4.5 nm, and then

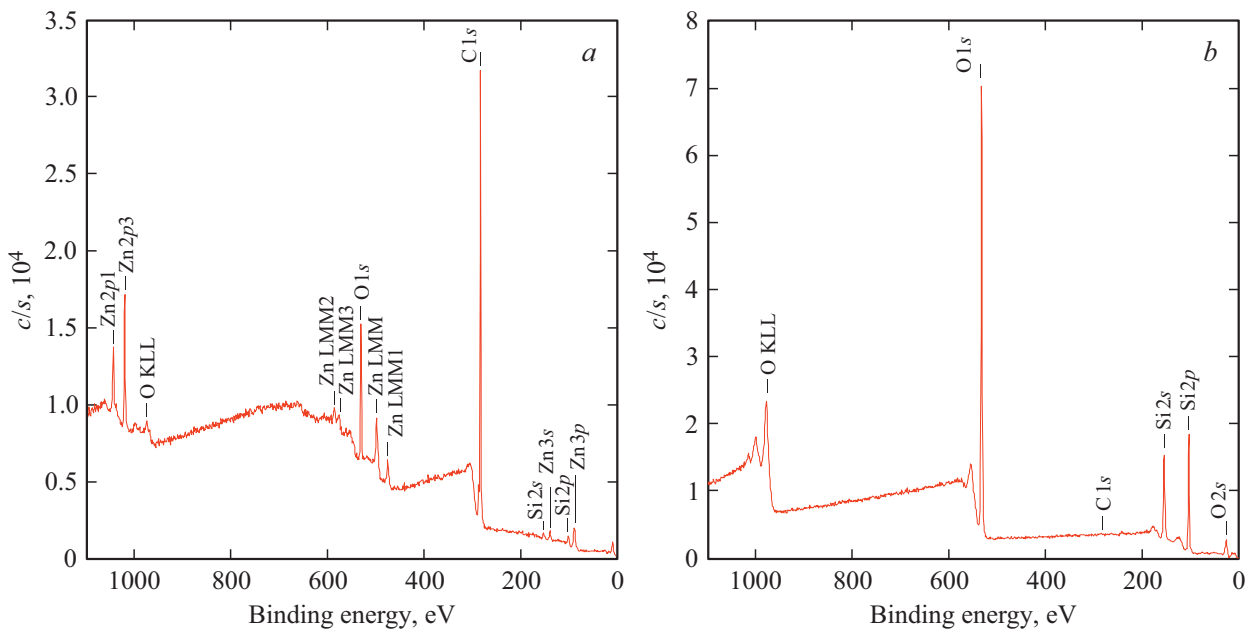


Figure 5. Survey XPS/AES spectra of the surface (0 nm) (a) and after 7 min etching (at depth of 63 nm) in the analysis region 1 (b).

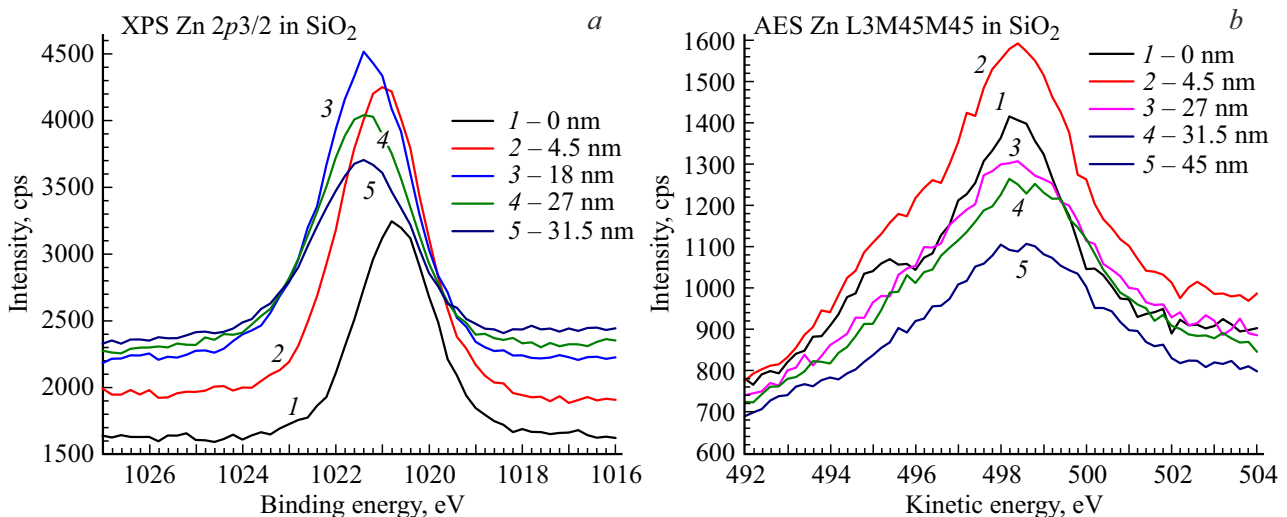


Figure 6. XPS-depth profiling spectra for the Zn2p_{3/2} (a) line and AES spectra for the Zn L3M45M45 (b) transition.

decreases in magnitude. It should be noted that the energy position of this Zn L3M45M45 Auger transition practically does not change with the depth of analysis and amounts to $E_{\text{kin}} = 498.4$ eV.

Figure 7, a shows high-resolution XPS- depth profiling spectra for O1s oxygen. It follows from this that the energy $E_B = 530.5$ eV corresponds to the XPS-signal maximum on the substrate surface. As the depth of analysis increases to 45 nm, the XPS signal increases and the position of its maximum shifts to the energy value $E_B = 531.8$ eV. An increase in the binding energy for the O1s line indicates a change in the charge state of oxygen towards an increase in its positive value, in other words, in the depth of the substrate, oxygen is in a stronger ionized state than on

the surface. In other words, if there is a loose structure with unsaturated bonds on the surface, in the depth of the silicon oxide matrix the bonds are already saturated and an equilibrium state corresponding to quartz is observed.

Figure 7, b shows high-resolution XPS- depth profiling spectra for Si2s silicon. It follows from this that the energy $E_{\text{sv}} = 152.0$ eV corresponds to the XPS-signal maximum on the substrate surface. As the depth of analysis increases to 45 nm, the XPS signal increases and the position of its maximum shifts to the energy value $E_B = 153.4$ eV. An increase in the binding energy for the Si2s line indicates a change in the charge state of silicon towards an increase in its positive value, in other words, in the depth of the substrate, silicon is in a more oxidized state than on the

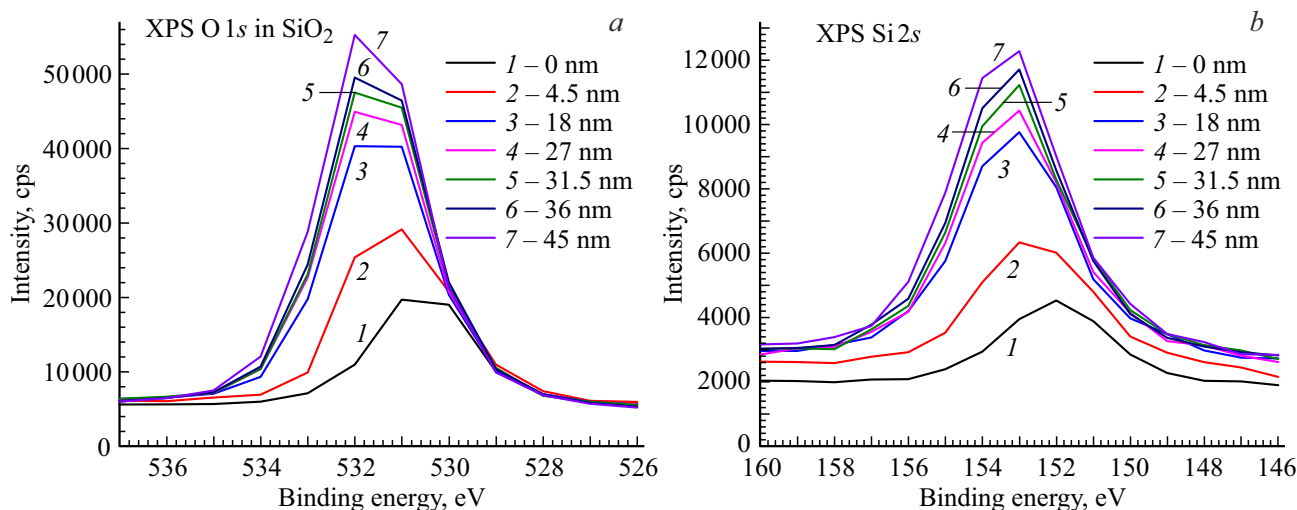


Figure 7. XPS-depth profiling spectra for the O1s (a) and Si2s (b) lines.

The concentrations of elements in the analysis region „1“ calculated using survey spectra before and after etching, and the Auger parameter (AP) $\alpha' = E(2p_{3/2}) + E(L3M45M45)$ for Zn

Etching time, min	d, nm	C1s at.%	O1s at.%	Si2s at.%	Zn2p3 at.%	α' , eV
0	0	37.5	40.5	11	9	2009.1 ± 0.4
0.5	4.5	14	52	25.8	1.5	2009.2 ± 0.4
1	9	2	58	31	1	2009.5 ± 0.4
1.5	13.5	0	61.5	31.5	0.5	2009.7 ± 0.5
2	18	0	62	32	2.0	2009.5 ± 0.5
2.5	22.5	0	63	32	2.5	2009.8 ± 0.5
3	27		64	32.5	3.0	2009.6 ± 0.5
3.5	31.5		63.5	32	4.5	2009.8 ± 0.4
4	36		65	32	2.5	2009.7 ± 0.5
4.5	40.5		65	33	2.0	2009.8 ± 0.5
5	45		66	33	1	2009.6 ± 0.4
5.5	49.5		66	33.5	0.5	2009.4 ± 0.5
6	54		67	33	0	
7	63		67	33	0	

surface. In other words, since the surface structure of the sample is rather loose with unsaturated bonds, the bonds are already saturated in the depth of the silicon oxide matrix and an equilibrium state corresponding to quartz is observed.

The concentrations of elements calculated using the above survey XPS-spectra, as well as using other survey spectra for this area at other depths, are given in the table.

To determine the concentration distribution profiles of elements over the sample depth, their profiles were measured with a step of 0.5 min for a total etching time of 7 min. According to the results of this measurement, it was determined that the Zn maximum corresponds to an etching time of 3.5 min, which corresponds to a depth of 31.5 nm (see Fig. 7). Then we studied the concentration profiles of elements in two other areas of the sample. The

etching times in them were selected as follows: 0.5, 2, 3, 3.5, 5, 7 min. The nature of the element distribution over depth in these regions of the sample surface differed significantly from the distribution in the first region (Fig. 7). Thus, at a depth of 31.5 nm, (3.5 min of etching), which corresponds to the maximum Zn concentration in the first region, there is no local maximum of zinc concentration in them, and the zinc content in these regions decreases with increasing etching time (with sample depth) much slower than in the first region. The zinc concentration maxima in these regions are observed near the surface, although the total zinc dopant content in them is the same. In other words, there is heterogeneity in the zinc distribution over the sample surface.

Focusing on the Auger parameter α' and based on the table data (right column), it should be noted that Zn in the SiO₂ film under study is in the charge state 1⁺ or 2⁺. In other words, Zn in the film is in the oxidized state in a mixture of Zn₂O · ZnO phases. For metallic zinc Zn⁰ we obtained the value of the Auger parameter $\alpha' = 2013.7$ eV. In the NIST [13] database, the values of the Auger parameter $\alpha' = 2009.5$ –2011.0 eV are given for ZnO. Using the XRD method for similar samples, we previously established [14] that Zn NCs with the (002) orientation and/or NCs of the ZnO (101) phase with the wurtzite structure, as well as NC of ZnO (111) with a cubic structure of zinc blende are formed in the SiO₂ film. The size of the coherent scattering region, calculated by the Debye–Scherrer formula [15], was 50 nm.

3.3. Study of current-voltage characteristics of structures

On annealed silicon oxide films containing NCs with a ZnO phase, C-V characteristics with a hysteresis loop were obtained for planar electrodes. One of these characteristics

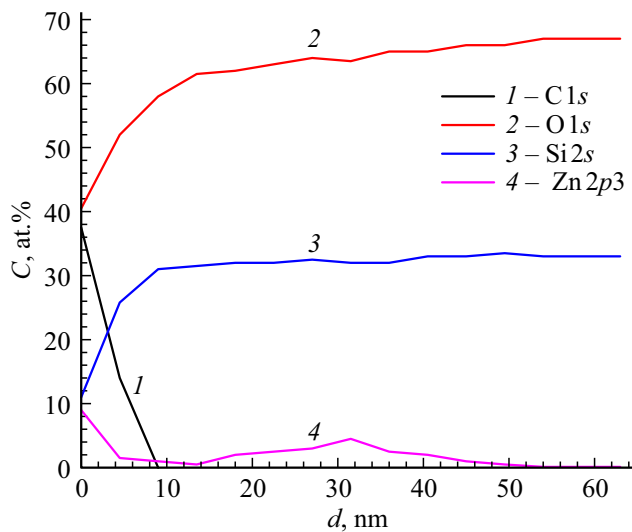


Figure 8. Profiles for the distribution of elements over depth.

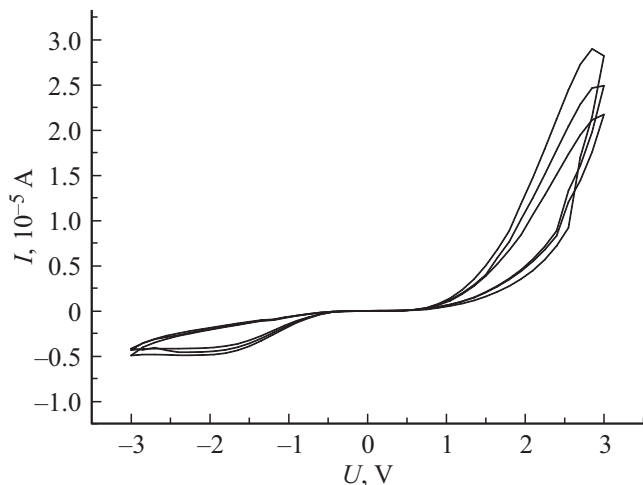


Figure 9. CVC characteristics of samples with planar contacts.

is shown in Fig. 9. This figure shows that the C-V characteristic has hysteresis for both polarities of the voltage applied to the sample. Since the C-V characteristics studies were carried out at room temperature, the possible mechanisms of charge transfer in our case can be currents limited by the space charge, hopping conduction, and the Poole-Frenkel mechanism [16]. It is currently difficult to determine the exact mechanism of charge transfer, since additional studies are required for material itself, in particular, to establish the structure of trapping levels in the obtained SiO₂ films doped with zinc, and for their role in formation of C-V characteristics of the obtained films with hysteresis effect. Note that with decreasing voltage on the sample, the current decreases, taking on larger values than with increasing voltage. This may indicate that, as the voltage increases, charge carriers are captured at deep recombination levels associated with the presence of Zn-containing clusters in the sample.

3.4. Discussion

The conducted experiments and measurement results confirm the predominant influence of process methods and specific modes of deposition of the active medium of memristor structures on their properties. Even under vacuum conditions, an internal mechanism for the heterogeneous layer formation manifests itself, which can greatly affect the reproducibility and stability of the electrical parameters of memristors. Simultaneous application of AFM and XPS spectral measurements and their comparison enables to assess the state and modification of the active medium of memristors, their dependence on methods and deposition modes, and to use it in the search for optimal process conditions.

One can try to improve the stability of the active medium of memristors by using low-temperature (up to 300°C) annealing in inert/neutral or active (oxidizing or reducing) media. It is necessary to study the effect of deviations from the stoichiometric composition of the memristor active medium on its structure and impurity doping that enables to create additional oxygen vacancies, which, as is known from most of the literature, are the main factor that forms the conducting channel (filament) that determines memristor operation. It is also possible to use electrodes made of metals that are oxygen getters, which will also contribute to the generation of oxygen vacancies in the near-surface layer of the memristor active medium. From our point of view, the most promising method for depositing the memristor active medium layers may be the method of reactive magnetron sputtering, which provides uniform distribution of elements over the sample surface and good reproducibility of the parameters of the deposited layers.

It should be noted that many process methods of film deposition are associated with the high-energy effect of electron and ion irradiation on the resulting layers during their formation. In this regard, it is also possible to use the ion doping method for the implantation of various impurities, in particular, zinc. Based on the theory of conducting channels, it can be concluded that they can be formed already in the memristor manufacture process. Modification of these filaments before their formation can be carried out by irradiating the memristor active medium with fast heavy ions [17], since such irradiation is known to lead to elongation in the direction of irradiation of metal and metal oxide (rarely) nanoparticles in various solid-state substrates [18]. Such irradiation can provide an additional positive effect in the formation of conductive filaments in metal oxide films of the active medium in ReRAM memory devices.

4. Conclusions

1. SiO₂ films doped with zinc with a thickness of 100–120 nm were obtained by the method of electron-beam evaporation and subsequent annealing in oxidizing atmosphere.

2. After deposition of a zinc layer on the samples surface, Zn-containing particles with an average height of about 25 nm and in-plane size of about 100 nm were fixed.

3. After annealing the structure in an oxidizing medium at 400°C for 30 min, the height of the particles on the film surface decreased to 12 nm, and their in-plane size increased to 100–200 nm.

4. Clusters on the sample surface consist of silicon dioxide containing a zinc impurity.

5. On the film surface after annealing in the Kelvin mode, particles of metallic zinc with an average size of 166 nm are fixed.

6. XPS/AES studies have shown that both on the surface of the silicon oxide film and in its depth, zinc is in the oxidized state to one extent or another.

7. For silicon oxide films doped with zinc annealed at 400°C, C-V characteristics with a hysteresis effect were obtained.

Funding

The work was carried out in FSI FSC SRISA RAS within the scope of the state assignment for conducting fundamental scientific research on the topic „Investigation of neuromorphic big data processing systems and their manufacturing technology“ No. FNEF-2022-0003 and partly the research was carried out using the equipment of the Research Equipment Sharing Center „Materials Science and Metallurgy“ at National University of Science and Technology „MISIS“ within the scope of the project No. 075-15-2021-696.

Conflict of interest

The authors declare that they have no conflict of interest.

References

- [1] J.J. Yang, D.B. Strukov, D.R. Stewart. Memristive devices for computing. *Nature Nanotechnology. Supplementary Information* (2013). www.nature.com/naturenanotechnology.
- [2] S.K. Tripathi, R. Kaur, M. Rani. *Solid State Phenomena* **222**, 67 (2015).
- [3] *Advances in Memristors, Memristive Devices and Systems / Ed. S. Vaidyanathan, C. Volos. In: Studies in Computational Intelligence Springer Ser.* **701** (2017).
- [4] U. Russo, D. Ielmini, C. Cagli, A. Lacaita. *IEEE Trans. Electron Dev.* **56**, 186 (2009).
- [5] M.H. Lee, K.M. Kim, G.H. Kim, J.Y. Seok, S.J. Song, J.H. Yoon, C.S. Hwang. *Appl. Phys. Lett.* **96**, 152909 (2010).
- [6] W. He, H. Sun, Y. Zhou, K. Lu, K. Xue, X. Miao. *Sci. Rep.* **7**, 10070 (2017).
- [7] C.W. Litton, T.C. Collins, D.S. Reynolds. *Zinc Oxide Material for Electronic and Optoelectronic Device Application*. Wiley, Chichester (2011). 386 p.
- [8] K.-C. Chang, T.-M. Tsai, R. Zhang, T.-C. Chang, K.-H. Chen, J.-H. Chen, T.-F. Young, J.C. Lou, T.-J. Chu, C.-C. Shih, J.-H. Pan, Y.-T. Su, Y.-E. Syu, C.-W. Tung, M.-C. Chen, J.-J. Wu, Y. Hu, S.M. Sze. *Appl. Phys. Lett.* **103**, 083509 (2013).
- [9] J.-S. Huang, W.-C. Yen, S.-M. Lin, C.-Y. Lee, J. Wu, Z.M. Wang, T.-S. Chin, Y.-L. Chueh. *J. Mater. Chem. C* **2**, 4401 (2014).
- [10] C.Y. Jiang, X.W. Sun, G.Q. Lo, D.L. Kwong, J.X. Wang. *Appl. Phys. Lett.* **90**, 263501 (2007).
- [11] C. Li, Y. Yang, X.W. Sun, W. Lei, X.B. Zhang, B.P. Wang, J.X. Wang, B.K. Tay, J.D. Ye, G.Q. Lo, D.L. Kwong. *Nanotechnology* **18**, 135604 (2007).
- [12] Department of Nanometrology, Czech Metrology Institute (<http://www.gwyddion.com>).
- [13] NIST X-ray Photoelectron Spectroscopy Database. Version 4.1. <http://srdata.nist.gov/xps>.
- [14] V.V. Privezentsev, A.P. Sergeev, A.A. Firsov, E.E. Yakimov, D.V. Irzhak. *Crystallography Rep.* **66**, 6, 1090 (2021).
- [15] *Handbook of X-Ray Photoelectron Spectroscopy / Ed. J. Chastain. Perkin-Elmer Corporation, Minnesota* (1996).
- [16] M. Lampert, P. Mark. *Injection currents in solids*. Mir, M. (1973), 416 p.
- [17] C. D'Orleans, J. Stoquert, C. Estourne's, C. Cerruti, J. Grob, J. Guille, F. Haas, D. Muller, M. Richard-Plouet. *Phys. Rev. B* **67**, 220101R (2003).
- [18] F.F. Komarov, O.A. Milchanin, V.A. Skuratov, M.A. Mokhovikov, A. Janse Van Vuuren, J.N. Neethling, E. Wendler, L.A. Vlasukova, I.N. Parkhomenko, B.N. Yuvchenko. *Bull. Russ. Acad. Sci.: Physics* **80**, 160 (2016).